REPORT DOCUMENTATION PAGE

Form Approved
OMB No. 0704-0188

1. REPORT DATE *(DD-MM-YYYY)*	2. REPORT TYPE	3. DATES COVERED *(From - To)*
31-08-2006	Journal Article	

4. TITLE AND SUBTITLE

Wave Front Sensor for Solar Concentrator Control (Postprint)

5a. CONTRACT NUMBER

5b. GRANT NUMBER

5c. PROGRAM ELEMENT NUMBER

6. AUTHOR(S)
Joseph N. Beasley (AFRL/RZSO)

5d. PROJECT NUMBER
10110062

5e. TASK NUMBER

5f. WORK UNIT NUMBER

7. PERFORMING ORGANIZATION NAME(S) AND ADDRESS(ES)

Air Force Research Laboratory (AFMC)
AFRL/RZSO
8 Draco Drive
Edwards AFB CA 93524-7135

8. PERFORMING ORGANIZATION REPORT NUMBER

AFRL-PR-ED-JA-2006-299

9. SPONSORING / MONITORING AGENCY NAME(S) AND ADDRESS(ES)

Air Force Research Laboratory (AFMC)
AFRL/RZS
5 Pollux Drive
Edwards AFB CA 93524-7048

10. SPONSOR/MONITOR'S ACRONYM(S)

11. SPONSOR/MONITOR'S NUMBER(S)
AFRL-PR-ED-JA-2006-299

12. DISTRIBUTION / AVAILABILITY STATEMENT

Approved for public release; distribution unlimited (AFRL-ERS-PAS-2006-223)

13. SUPPLEMENTARY NOTES
Published in IEEE Transactions on Aerospace and Electronic Systems, Vol. 45, No. 4, October 2009.

14. ABSTRACT

This article is the culmination of research directed into finding a system to control the position of the focal spot of paraboloid concentrators for use in terrestrial and space solar concentration applications. After a brief introduction into the area of study, the article describes how a normal Shack-Hartmann wavefront sensor is modified for use in detecting and tracking the focal spot. The first experiment describes how the wavefront sensor is to be utilized in a solar application and shows the adjustment from lenslets to cylindrical mirrors on a thruster. Next, the paper details the analysis and development of the algorithms used in locating the focal spot on a thruster absorber utilizing a correlation method and an area centroid method. The article concludes with a paragraph on suitable future work.

15. SUBJECT TERMS

16. SECURITY CLASSIFICATION OF:			17. LIMITATION OF ABSTRACT	18. NUMBER OF PAGES	19a. NAME OF RESPONSIBLE PERSON
a. REPORT	b. ABSTRACT	c. THIS PAGE			Dr. Michael R. Holmes
Unclassified	**Unclassified**	**Unclassified**	A	14	19b. TELEPHONE NUMBER *(include area code)* N/A

Wave Front Sensor for Solar Concentrator Control (October 2007)

JOSEPH N. BEASLEY, Member, IEEE

MICHAEL R. HOLMES
U.S. Air Force Research Laboratory

HEN-GEUL YEH, Senior Member, IEEE
California State University, Long Beach

This article is the culmination of research directed into finding a system to control the position of the focal spot of paraboloid concentrators for use in terrestrial and space solar concentration applications. After a brief introduction into the area of study, the article describes how a normal Shack-Hartmann wave front sensor is modified for use in detecting and tracking the focal spot. The paper details the analysis and development of the algorithms used in locating the focal spot on a thruster absorber utilizing a correlation method and an area centroid method. The article concludes with a paragraph on suitable future work.

Manuscript received November 28, 2006; revised January 2, 2008; released for publication June 9, 2008.

IEEE Log No. T-AES/45/4/934232.

Refereeing of this contribution was handled by M. Ruggieri.

This work was supported by the U.S. Air Force Research Laboratory, Edwards AFB, CA.

Authors' addresses: J. N. Beasley, U.S. Air Force Research Laboratory, Experiment Demonstration Branch, Edwards, AFB, CA 93524, E-mail: (joseph.beasley@edwards.af.mil); M. R. Holmes, U.S. Air Force Research Laboratory, Spacecraft Branch, Edwards AFB, CA 93524; H-G. Yeh, Dept. of Electrical Engineering, California State University, Long Beach, Long Beach, CA 90840.

I. INTRODUCTION

For direct thrust solar thermal propulsion (STP) or terrestrial solar heating using concentrators, proper positioning of the solar focal spot is paramount. Along with positioning information, a sensor system must tolerate the intense heat generated by a solar concentrator. The sensor system developed in this article satisfies both of the previous requirements. The system developed in this article utilizes the thruster/absorber as the focal spot sensor with a charge coupled device (CCD) camera to image the absorber/sensor. Two image processing methods are applied to the CCD images to generate the focal spot location. Once the focal spot is located on an image, positioning information and commands are generated to reposition the concentrators. Both methods produce the focal spot information needed to generate positioning information for the concentrator.

This article is organized as follows: The STP background is presented in Section II. The solar sensor problem statement is discussed in Section III. Wave front sensors and cylindrical mirrors as applied to the problem statement are discussed in Section IV. Section V presents the first algorithm developed and applied to the model of the concentrator system; while Section VI presents the algorithms developed specifically for utilizing the wave front sensor. A summary and conclusion is given in Section VII.

II. SOLAR THERMAL PROPULSION BACKGROUND

The solar concentrator field may be divided into two primary areas of interest: terrestrial-based and space-based. Both types of concentrator can be either imaging or nonimaging and they can be rigid or inflatable. Other applications include terrestrial power, space power, materials processing, hazardous material destruction, building illumination, and space plant illumination.

Solar thermal power as propulsion has its roots in the work of Krafft Ericke's solar powered spaceship done in 1956. Ericke's spaceship was the first design that utilized a double solar concentrator connected together by a hydrogen powered thruster.

The major difference between a chemical-type thruster or spacecraft and an STP thruster or spacecraft is that the STP spacecraft does not carry the added weight of the oxidizer as the chemical spacecraft. Since the energy for propulsion is available to the spacecraft in orbit, in the form of sunlight, an STP system would not have to carry both propellant and oxidizer to produce energy for the upper stage unit. Only an atomic or molecular propellant such as hydrogen would be needed on the upper stage for thrust. Thus, the STP can have a weight advantage over the chemical spacecraft in that a lighter molecular weight propellant is used.

The STP system heats up hydrogen in the thruster/absorber and then expands the hydrogen through a nozzle to produce the thrust required by the vehicle. Thus the thrust-to-mass (propellant) efficiency of the STP system is much better (more than two times better) than the equivalent chemical upper stage as less nonpayload mass is needed in the STP system for the same amount of thrust to be developed. [1] Specific impulse or I_{sp} is the rocket propulsion term that measures the thrust per unit of propellant expended. Thus STP systems have a much higher I_{sp} than chemical systems of the same size.

The definition of I_{sp} is the thrust divided by the propellant expelled in the exhaust

$$I_{sp} = \frac{|\mathbf{F}|}{g_c \dot{m}} = \frac{1}{g_c \dot{m}} \left| \frac{d\mathbf{p}}{dt} \right| = \frac{1}{g_c \dot{m}} \dot{m} v_e = \frac{v_e}{g_c}. \tag{1}$$

In (1), v_e is the exhaust velocity. From (1), the expression for the power developed by the exhaust stream of the thruster is shown in (2)

$$P_e = \mathbf{F} \cdot \mathbf{v}_e = \tfrac{1}{2} \dot{m} g_c^2 I_{sp}^2. \tag{2}$$

Equation (2) can be related to concentrator power input P_{in} to the thruster and the thruster nozzle loss mechanism η_t as follows in (3)

$$P_e = \eta_t P_{\text{in}}. \tag{3}$$

The solar intensity at Earth is shown in (4)

$$I_0 = 1350 \frac{W}{m^2} \pm 50 \frac{W}{m^2}. \tag{4}$$

The power transferred to the thruster and gas is the intensity of the light collected by the concentrators minus radiation lost. The power into the thruster is then (5)

$$P_{\text{in}} = (I_{\text{in}} - \sigma A T^4). \tag{5}$$

In (5), σ is the Stefan-Boltzmann constant, I_{in} is the intensity from concentrator to absorber A, and T is the temperature of the absorber and propellant. In (5), I_{in} is input intensity with effects of the optical path through the concentrator acting on it as shown in (6)

$$I_{\text{in}} = \tau_c A_c I_0. \tag{6}$$

In (6), τ_c is the transmission efficiency of the concentrator system, A_c is the area of the concentrator aperture, and I_0 is the solar intensity at Earth orbit. Defining concentration ratio as $C_r = A_c/A$ with A as the area of the thruster/absorber face; then from (3), (5), and (6) the power at the exhaust stream is shown in (7)

$$P_e = \eta_t A(\tau_c C_r I_0 - \sigma T^4). \tag{7}$$

Equation (7) is a one-dimensional expression for the power into the thruster describing the first-order trade-off between concentration ratios and operating temperature. The assumptions for (7) are that the thruster has a uniform temperature over A, that the backside of A is insulated, and the temperature over A is the same for the propellant. Otherwise, (7) would become an integral over the flow path. Equation (2) and (7) may be used to find thrust F as a function of I_{sp}, T, and I_0.

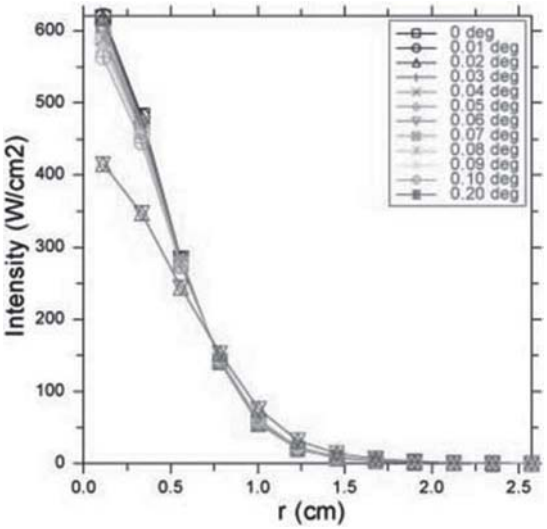

Fig. 1. Peak power density versus radius off focus.

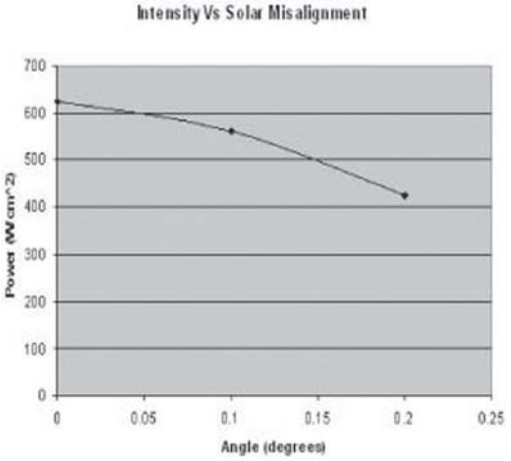

Fig. 2. Intensity versus solar misalignment.

Relating the exhaust power P_e to the misalignment angle of the concentrator is a problem solved numerically using the concentrator code written by Dr. Holmes called offaxis. Fig. 1 shows the result for several angles of misalignment. Using values from this Fig. 1, Fig. 2 plots the intensity versus misalignment angle. Fig. 2 shows that the power density decreases considerably at 0.2 deg of misalignment.

The peak power at 0.2 deg of misalignment is approximately 2 dB down and indicates a likely cutoff point for this discussion. Therefore, most of the work presented in this article pursued a 0.1 deg of misalignment target value for maximum power transfer to the thruster.

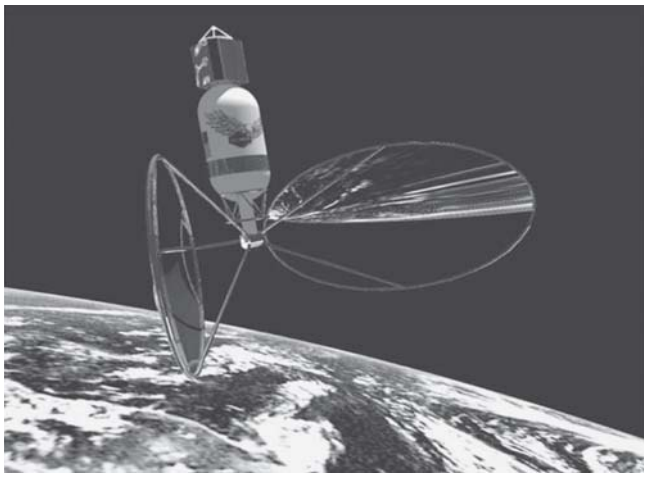

Fig. 3. Solar thermal configuration.

Misalignment is the difference between the position of the Sun and the position of the axis of symmetry of the paraboloid-shaped concentrator. Misalignment or alignment is really a matter of correctly positioning the focused beam from the approximately paraboloid concentrator onto the absorber so that maximum power is absorbed into the propellant. It is not changing the shape of the concentrator, but moving struts around in 3-D space to position the focal beam onto the thruster. A paraboloid reflector is a concave mirror whose cross-sections are parabolas or it can be described as a parabola rotated about its axis. This type of mirror can concentrate light at its focus and provide tremendous heat. However, to provide the most heat, the paraboloid must be accurately pointed.

Along with controlling the concentrator during thrusting operations, another control requirement is that the focal cone should always be positioned on the aperture closest to the nozzle for effective heat transfer to the propellant. [2] This positioning of the focal beam is determined by the misalignment of the concentrator with respect to the Sun, and with respect to the absorber.

Since the concentrator for this article is an inflatable style, the pointing information derived from the sensor designed in this article could be useful for providing another input to the inflation control unit to increase the accuracy of the paraboloid. This is a separate result that was not utilized for the current article.

The current Air Force Research Laboratory (AFRL) concept for the concentrators for a solar thruster is two off-axis paraboloid concentrators connected to a central thruster. See Fig. 3.

Each concentrator is connected to the central thruster with a hexapod or Stewart platform offering 6 degree of freedom (DOF) control. The 6 DOF needed are yaw, pitch, roll, x, y, and z. Coarse alignment brings the focal cone into rough alignment with the desired aperture on the thruster [2]. Coarse alignment is obtained using an on-axis detector, such as a Sun tracker or photodiode, which brings the spacecraft and concentrators into a general alignment with the Sun. Concentrator control should provide optimum energy transfer to the solar thruster while protecting the concentrator and spacecraft from the dynamic behavior of the whole system.

III. SOLAR SENSOR PROBLEM STATEMENT

To be useful as a solar sensor especially in space, the sensor cannot rely on Earth coordinates for tracking information. The sensor also must be able to handle the high temperatures involved with a solar concentrator that concentrates the sunlight to temperatures approaching 3100 K on the absorber.

The research problem is to: 1) develop a sensor that provides information about the location of the focus beam from the concentrator that also can tolerate the extreme temperatures involved in providing solar heating, and 2) develop the mathematics of a control system that will focus the concentrator in an optimal fashion based on the sensor measurements.

The sensor developed solves the temperature issue by using the absorber as a wave front sensor for focal spot determination. This sensor overcomes the thermal limitations of the other sensors by using the reflections of the concentrated light in the sensor as the tracking information. Since the absorber has to take the high temperatures of the concentrated sunlight, it is already capable of handling the temperature requirements. The CCD images the absorber to determine the location of the focal beam based on shape, size, and location of the reflections on the absorber. Additionally, the thrust could be monitored and used as a feedback mechanism to enhance the control of the focal spot.

IV. WAVEFRONT SENSOR

The Hartmann wave front sensor was developed by Hartmann in 1900 and was used for checking optical telescopes for aberrations. It was an array of holes in a plate placed in front of the mirror of the telescope being checked so that light tubes from the array would impinge on the telescope mirror. Two photographic plates were used to collect the light information. One plate was placed just before the focal spot of the telescope and the other one was placed just behind the focal spot. The distance between the plates was chosen so that the light rays would be separated from each other. The path of the light rays was traceable by measuring the centroids of the two images. Thus, Hartmann was able to determine figures of merit for various large telescopes [3].

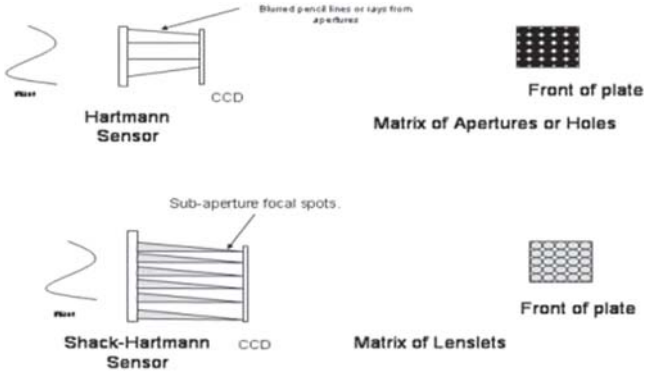

Fig. 4. Wave front sensor comparison.

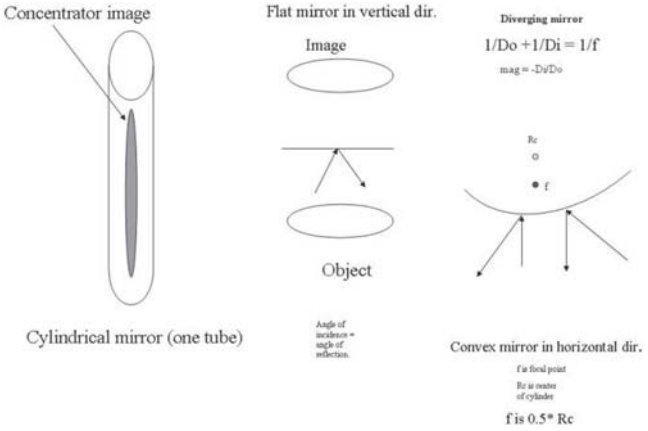

Fig. 5. Cylindrical mirror.

Dr. Roland Shack developed the method of replacing the holes of the Hartmann sensor with small lenses or lenslets to improve the capability of the Hartmann sensor when taking images of satellites or stars at the same time as the wave front phase error was being determined. The method was developed while solving a problem with imaging satellites and stars from the Earth. Dr. Aden Mienel's solution was to determine the optical transfer function of the atmosphere at the same time as the image being taken. The Hartmann sensor was not satisfactory as Mienel could not allow the array to cover the aperture of the telescope because it would eliminate the image of the satellite in favor of determining wave front tilt over the imaging of the satellites. Mienel tried to use a beam splitter to take Hartmann images while taking images of the satellites and stars. This method suffered from the weak intensity images of the light rays in the Hartmann sensor. Shack suggested that replacing the apertures in the Hartmann sensor with lenses would eliminate the problems that Mienel was having with his Hartmann device. The lenslets focused spots onto an image plane such that the displacement of the spots from the ideal position of the spots indicated wave front tilt [3]. Thus, the Shack-Hartmann system overcame the shortcomings of the Hartmann sensor while increasing the sensitivities of the Hartmann device alone. A comparison of the two systems is depicted in Fig. 4. The Shack-Hartmann sensor is not suitable for use in tracking the focal spot of concentrated solar rays because of the high temperatures encountered in a concentrated sunlight application. As with other sensors, lenslets would suffer from the effects of concentrated light and from contamination of hot absorber vapors.

The wave front sensor described in this article utilizes the tubing of the absorber as mirrors that collect information about the light scattered on the sensor from the concentrator. In this manner, the tubes take the place of the holes or lenslets of the Hartmann or Shack-Hartmann wave front sensor.

The tubes from the conical absorber act like cylindrical mirrors (torroidal mirrors) in reflecting the sunlight from the concentrator to the CCD. The virtual location is important in applying the principles from wave front sensing, since the CCD array cannot physically be located behind the mirrors or tubing. In the current case, the lens system virtually or mathematically positions the array behind the absorber in a manner similar to the Shack-Hartmann system. Each tube would have its own corresponding subset of virtual pixels mapped directly onto the CCD array. These subsets would not overlap. Fig. 8 shows the schematic of the thruster and concentrator with a view of the light in the concentrator as seen by the tubes of the absorber.

A. Cylindrical Mirrors

Since the sensor for this application uses coiled tubing as its primary configuration, a brief review of cylindrical mirrors is necessary to understand the reflections generated by the conical tubing absorber. Fig. 5 shows the normal situation encountered with the use of a cylindrical mirror. In general a cylindrical mirror will tend to compress an object's reflection along the length of the mirror. An object's reflection also tends to get larger as the object moves towards the mirror.

Fig. 5 also shows the reflections from the cylindrical mirror along two of its axes. In one axis, in the straight on view, the cylindrical mirror acts like a flat mirror with the light rays adhering to the rules for a flat mirror. That is, incident light is reflected such that the reflected ray returns from the mirror as if it originated at a point behind the mirror, at equal distances to the object; this is also a virtual image. Or the reflection occurs such that the reflected ray's angle is equal to the angle of the incident ray. On the other axis of the mirror, reflections follow the rules of a convex mirror. That is, the mirror surface has a virtual focus point and all of the reflected light rays appear to come from that focus point behind

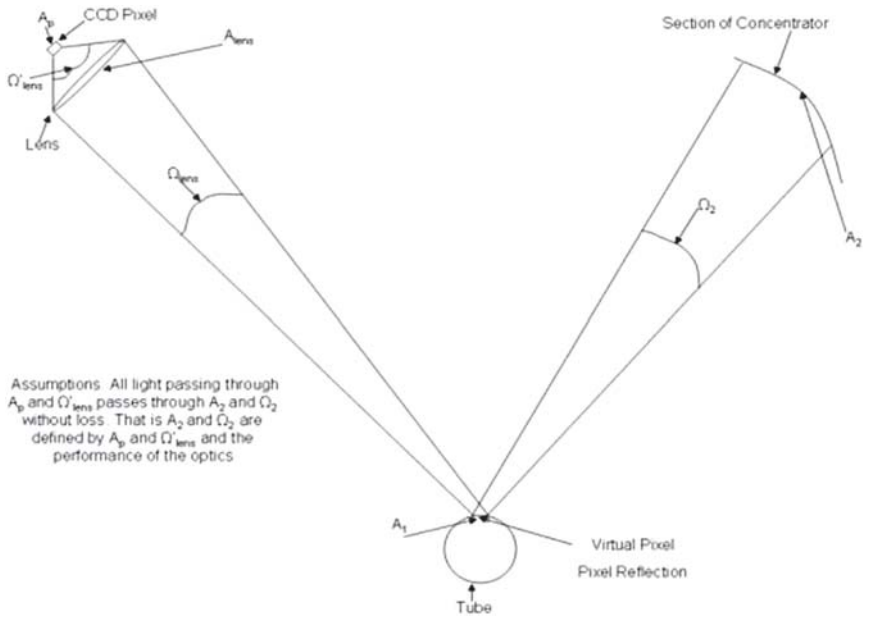

Fig. 6. Flux tube constructions.

the mirror surface. Reflections from other portions of the cylindrical mirror are more complex than the reflections just discussed, however, the overall effect is that the reflection in the cylindrical mirror is compressed along its main axis and appears larger as the viewer moves closer to the mirror.

B. Flux Tube Calculation

The flux tube construction shown in Fig. 6 was used to determine the ability of the CCD pixels to discern changes in light on the concentrator due to misalignment via the sensor mirrors. A concentrator that is on focus would have light filling all of the concentrator as seen by an observer located at the focus. The sensor or observer in the present case is the absorber/sensor developed in this article.

Since we assume that we don't lose light from the flux tubes, then the pixels should see the same intensity from the tube path as it sees looking directly at the Sun. Also, we assume that our optical system is perfect without any loss of light from the flux tubes due to transmission losses or reflection losses. The construction presented in Fig. 6 illustrates that with perfect optics, the light intensity on a pixel via the concentrator mirror path is identical to the light intensity that the pixel would receive by direct viewing of the Sun. All virtual pixels whose solid angle fell within the 30 deg half-angle of the cone would have full intensity light on them. Therefore, any pixel intensity value less than direct Sun intensity and whose solid angle fell within the cone of light of the concentrator would indicate misalignment of the concentrator. If the pixel was at or beyond the angle of the cone of the concentrator, that pixel would then be considered a border pixel and would not have full intensity.

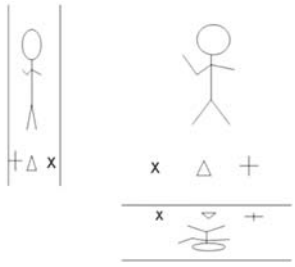

Fig. 7. View of figures in cylindrical mirror from camera.

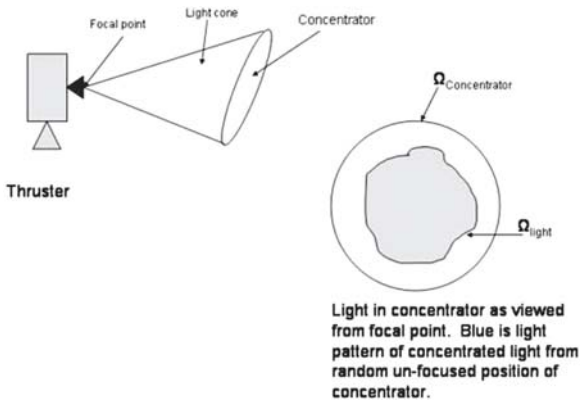

Fig. 8. Light in concentrator.

Fig. 7 shows a schematic of the camera view of the image of the symbols and stick figure formed by the cylindrical mirrors of the tubing with the CCD of the plane of the symbols. While Fig. 8 indicates how a CCD matrix would view the reflection of the concentrator in the tubing.

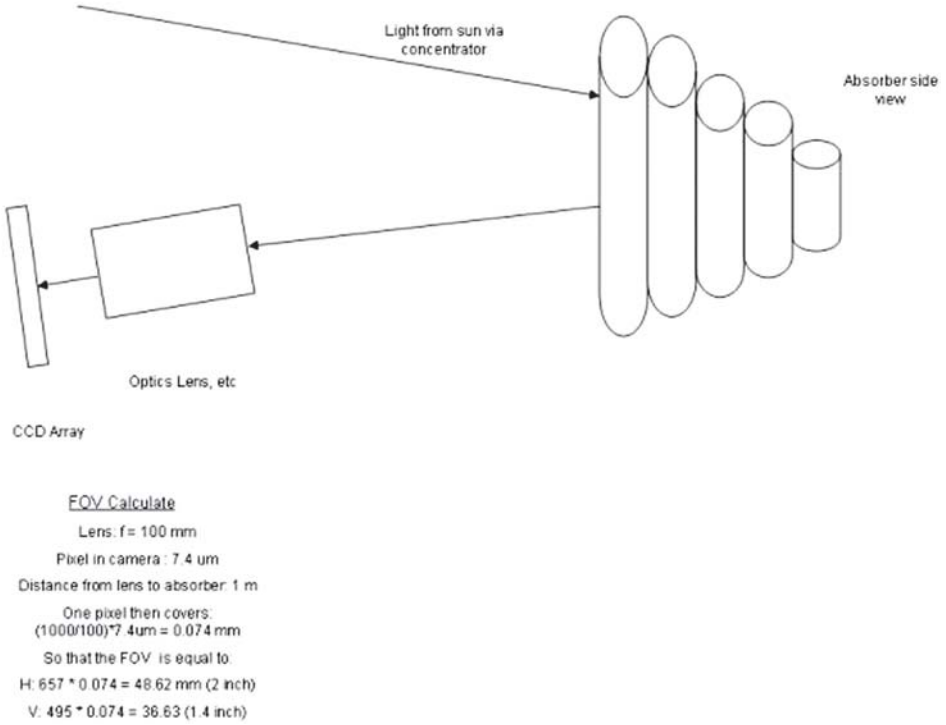

Fig. 9. Schematic of proposed solution.

V. MODEL SENSOR CALCULATIONS

A. Methods

Each image taken could be processed by utilizing profile information along diagonal lines representing the four quadrants of the circle (along the 45 deg angles, say). The areas of maximum intensity would be determined along each profile line. The maximums should occur roughly where the tubes appear in the image as that is where pixel virtual images are located. The difference between these areas should give an indication of the direction to the focal spot (almost a centroiding operation on the maximum areas in the image).

By knowing where the center of the absorber is located with respect to the camera (a nontrivial assumption as the camera would probably be mounted to one of the concentrator's movable struts), the controller should be able to generate x, y, z, roll, pitch, and yaw commands for the hexapod controller to move the concentrator to a new position to provide better focus and thus better heating. Fig. 9 shows the schematic of the proposed sensor solution.

For the development of the model presented in this article, a copper conical absorber with water-cooling if needed is used. Fig. 10 presents the water-cooled conical-shaped absorber as shown in the schematic in Fig. 9. The fluid to be heated flows through the absorber tubing and is heated by the concentrated light.

Fig. 10. Conical absorber sensor.

B. Calculations

Ray tracing was used to determine whether the image of the 7 in diameter concentrator model would reflect off of the tubes and into the aperture of the CCD camera. Fig. 11 illustrates the situation and the equation shown could be used in an iteration to find the angular extremes that would in fact be imaged in the CCD camera. The figure indicates a theta angle that would in fact be double the angle with respect to the normal vector at the surface of the cylinder. This is happening because of the way things were drawn in Fig. 11 and the Law of Reflection: the angle of incidence is equal to the angle of reflection. A quick calculation using just the rays from the extremes of the concentrator model using the Law of Reflection

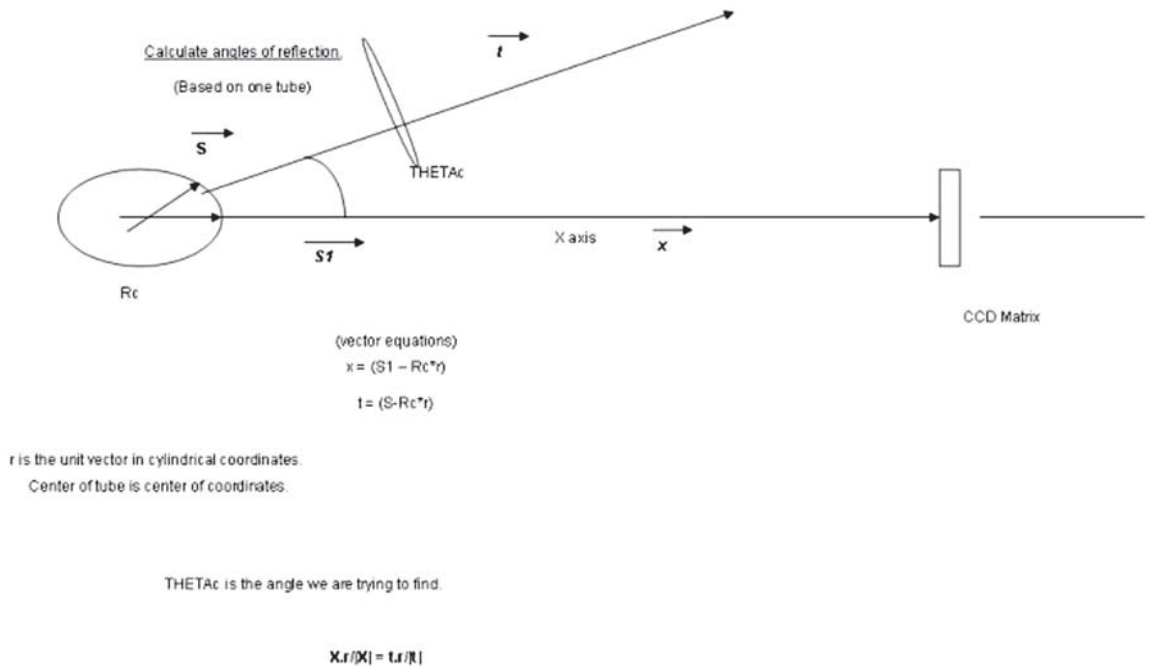

Fig. 11. Vector calculation for reflection in CCD.

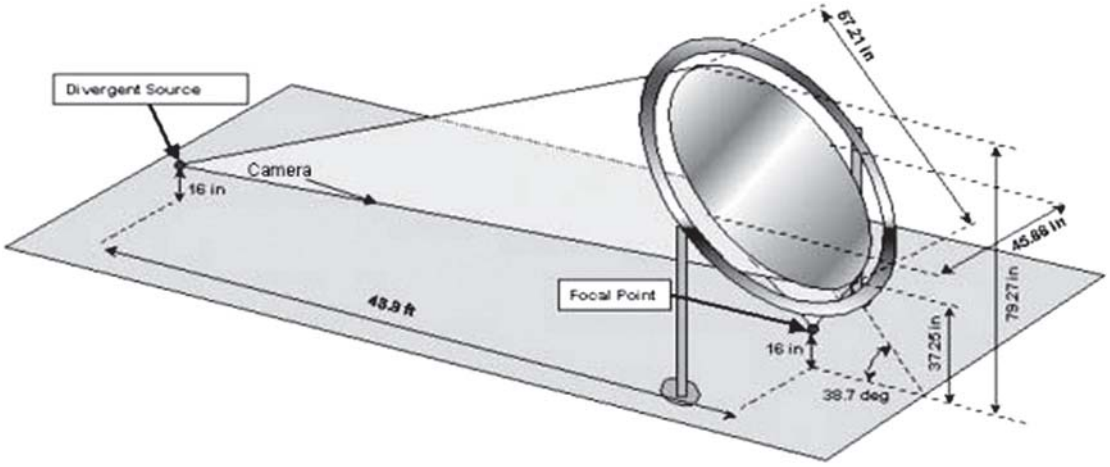

Fig. 12. Test apparatus setup.

showed that the CCD matrix or camera was able to view all of the reflection of the concentrator model from the tubes.

The field of view of the CCD camera was determined to be 1.4 (495 rows) $\times$ 2 (657 columns) in at a distance of 1 m from the tubes.

VI. WAVE FRONT ALGORITHM DEVELOPMENT

Since the paper [4] presents the hardware being used for focal spot tracking in detail, a brief summary of the components is now presented for use in this article. The schematic of the hardware is shown in Fig. 12 and consists of a CCD camera, 1×2 m elliptical concentrator and a conical-shaped tubular absorber. A simulator consisting of a 3 in diameter LED taillight was used to represent the Sun's disk at the Earth's orbit for the 1×2 m concentrator shown in Fig. 12. The actual value of the solar disk at Earth's orbit is 5 in so the 3 in disk in the simulation actually provided a more stringent requirement than the operational STP system. The Sun simulator was mounted on a tripod that allowed various movements of the Sun from on focus to 3–4 diameters off of on focus for imaging and analysis. Putting the Sun simulator at the second focus of the concentrator allowed for simulation of the overall STP system in a laboratory environment using various misalignments off of the second focus point situations to be simulated.

The developed algorithms are based on the Shack-Hartmann wave front sensor. The holes and lenslets are replaced by the cylindrical mirrors of the absorber in the current system. Sunlight reflecting

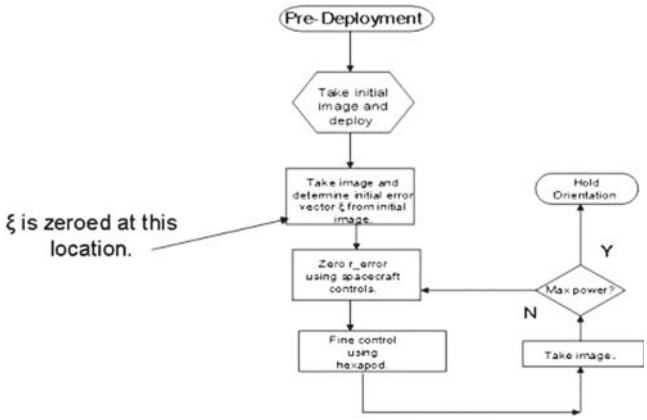

Fig. 13. Flow chart of sequence.

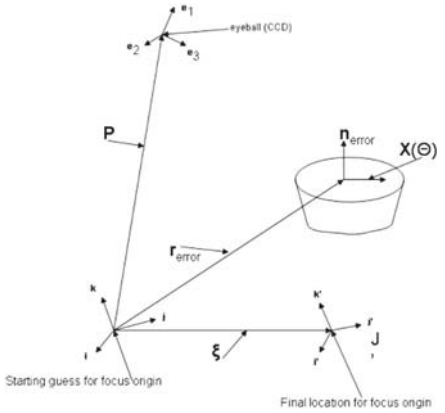

Fig. 14. Coordinate system after deployment.

on the absorber tubing is imaged by the camera for analysis instead of imaging the array of holes or lenslets of the Shack-Hartmann device. The thruster tubes serve as high temperature mirrors. The absorber takes the heat from the sunlight and conducts it to the hydrogen gas for use in providing thrust. Differences in location of light and how much light is reflected from the tubes are used to determine the focal spot location error for use in a feedback control system.

Two or more different tracking algorithms are used to locate the focal spot location from the images of the tubes. Different algorithms were deemed necessary because of the 0.1 deg arbitrary control requirement and not having one universal algorithm that covered the three regimes of focus coarse focus (sunlight more than 5 diameters off focus), intermediate focus (approximately 5–3 diameters off focus), and fine focus (2–0 diameters off focus).

A. Method One

The first method to be discussed is the more general method using correlation, while the second method is less general, based on area moments and area centroids similar to one version of the Shack-Hartmann analysis. The flow chart in Fig. 13 shows the sequence to be implemented for solar concentrator focus control. Fig. 14 illustrates the situation for the spacecraft just after deployment. The coarse focus control system operates on the vector positioning the systems so as to minimize this vector. The situation then is shown in Fig. 15. The focal spot is located in the general area of the sensor but not on the optimized spot and that the system is not thrusting. Thus, after deployment and coarse alignment, the camera is pointed at the absorber and the concentrator is positioned facing the Sun. This situation is then defined as the initial position for the fine focus control algorithms. With the addition of a stored image of the absorber in the on-Sun and on focus designed configuration, the control algorithms begin.

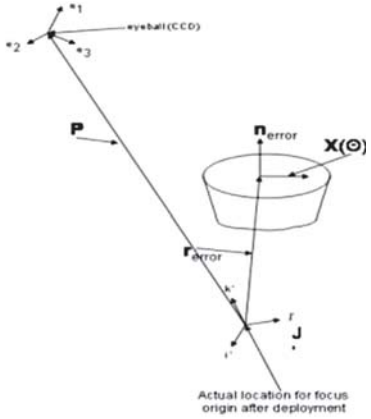

Fig. 15. Coordinate system, fine focus control.

At the start of the control program, the control computer has this initial configuration and initial image in memory. Also stored in the control computer are masks to be used in computing where the focal spot is currently located each iteration. The correlation or the lack of correlation at the masked areas indicates the current location of the spot and provides the direction of travel required to reduce the mismatch. The overall process for this control algorithm follows image correlation or scene matching from computer pattern recognition [5–7].

From Fig. 15, $\mathbf{r}_{\text{error}}$, $\mathbf{p}$, $\mathbf{X}(\theta)$, and $\mathbf{n}_{\text{error}}$ are the primary vectors in the development of the algorithms. $\mathbf{r}_{\text{error}}$ is the vector that determines the location of the image in both coordinate systems for the focus spot and is the vector to be minimized in the fine focus algorithms. $\mathbf{n}_{\text{error}}$ is the vector normal to the plane at the current image location at $\mathbf{r}_{\text{error}}$. $\mathbf{p}$ is the location of the camera or "eye-position" with respect to both coordinate systems. Finally, $\mathbf{X}(\theta)$ is defined as the vector representing areas of the images that are located in regions of interest. The regions of interest in the case of these algorithms would be the thruster itself or the individual rings of the absorber. The required accuracy of focal spot location determines whether the thruster as a whole

would be the region of interest or the individual rings.

For the imaging portion of the process, the vector $\mathbf{X}(\theta)$ in the preceding paragraph would have to be projected onto the CCD camera image plane. The method used for this operation is based on pinhole optics and projection. The CCD camera utilizes a pinhole-like aperture larger than a pixel for its near infinite depth of field. A lens is positioned just behind the pinhole-like aperture to focus the aperture image onto the CCD matrix in the camera. With these optical parameters the projection of $\mathbf{X}(\theta)$ onto the CCD matrix with coordinates (a,b) is determined using the following equations

$$a(\theta) = \alpha * ((\mathbf{X}(\theta) + \mathbf{r}_{\text{error}} - \mathbf{p}) \cdot \hat{e}_1)/(\mathbf{X}(\theta) + \mathbf{r}_{\text{error}} - \mathbf{p}) \cdot \hat{e}_3 \tag{8}$$

$$b(\theta) = \beta * ((\mathbf{X}(\theta) + \mathbf{r}_{error} - \mathbf{p}) \cdot \hat{e}_2)/(\mathbf{X}(\theta) + \mathbf{r}_{error} - \mathbf{p}) \cdot \hat{e}_3. \tag{9}$$

The parameters α and β in (8) and (9) are scaling factors determined by the CCD pixel size. The $\hat{e}$ vectors are unit vectors located at $\mathbf{p}$ defining a coordinate system at $\mathbf{p}$ for the camera.

Now that the image and system coordinates and vectors have been defined, the correlation function is derived. The image taken by the CCD is denoted $I(a,b)$ and is a function of (α,β) as expected. $W(\alpha,\beta)$ will represent the image or subimage that we are trying to match. For example, $W(\alpha,\beta)$ would represent the ideal on focus image or it could represent only a portion of the ideal image such as specific rings of the sensor. The L_2 norm is then utilized to calculate the minimum distance between $W(\alpha,\beta)$ and the current image

$$E(m,n) = \left(\sum_{i=1}^{I} \sum_{j=1}^{J} [I(i+m-1, j+n-1) - W(i,j)]^2 \right)^{0.5}. \tag{10}$$

Where $E(m,n)$ in (10) is the measure of distance at coordinates (m,n). Equation (10) also assumes that W is smaller than the image I, but that does not preclude using a W that is equal to I in size. Square and expand both sides of (10) while using the assumption that the energies in W and I are constant and very small; the correlation of W and E results as shown in (11)

$$E^2(m,n) = -2 * \sum_{I=1}^{I} \sum_{J=1}^{J} I(i+m-1, j+n-1) * W(i,j). \tag{11}$$

Multiplying (11) by $-1/2$ generates the correlation $R(m,n)$ at (m,n) as shown in (12)

$$R(m,n) = \sum_{i=1}^{I} \sum_{j=1}^{J} I(i+m-1, j+n-1) * W(i,j). \tag{12}$$

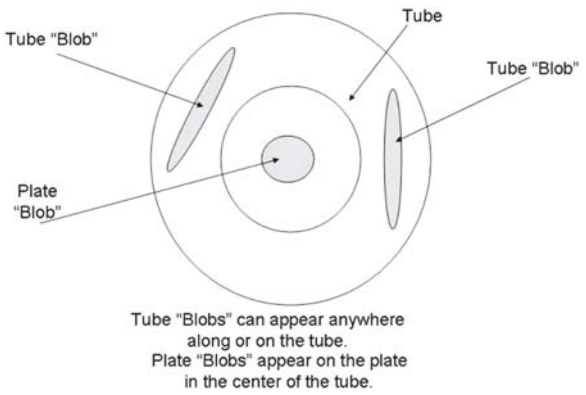

Fig. 16. Generic light images on tubes of sensor.

Finding the maximum value for $R(m,n)$ determines the best location in the image that matches W. Finding the X,Y location of the maximum value for $R(m,n)$ and determining the difference from that location to the location of the autocorrelation of the on focus image determines which direction to move the image. Once the difference between the autocorrelation of the on focus image location and the point of maximum correlation is found, the control system would move the concentrators to reduce this difference. Equation (12), correlation, was thought to be sufficient for determining the location of the focus.

B. Method Two

The second method for determining focal spot location is by measuring light area moments in the image. This method is derived based on a modification of the Shack-Hartmann wave front sensor using cylindrical mirrors instead of lenslets to register light areas [9]. Images of the concentrator can be seen in each coil of the absorber. Whether a particular image on the tube, denoted as a "tube blob" is bright or dim depends on how close the tube is to the focal point. An image area moment using the "tube blob" areas is calculated to find the focal location. The derivation also follows from a discussion of area moments and centroids from mechanics [10].

Fig. 16 shows a generic schematic of light blobs from an image of the sensor. The shape and intensity area of each tube blob is related to the amount of light in the concentrator being directed to that area of the tube. Calculating the area centroid of the images in the tubes determines where the focal spot is located on this iteration of the algorithm. Knowing where the centroid of the focal spot is located for this iteration determines in which direction the control algorithm needs to move the concentrator, to move the centroid to the center of the sensor.

Fig. 17 shows the situation that might occur once the CCD acquires an image. A coordinate system for the image is shown in Fig. 17. The image is then

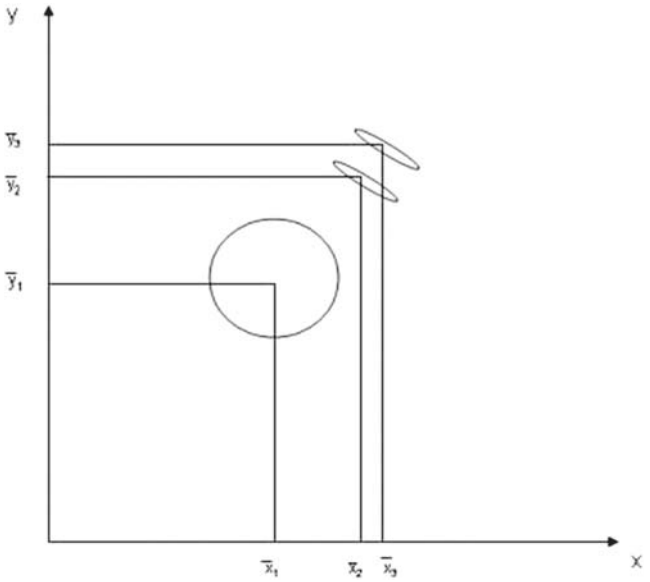

Fig. 17. Light in image from CCD.

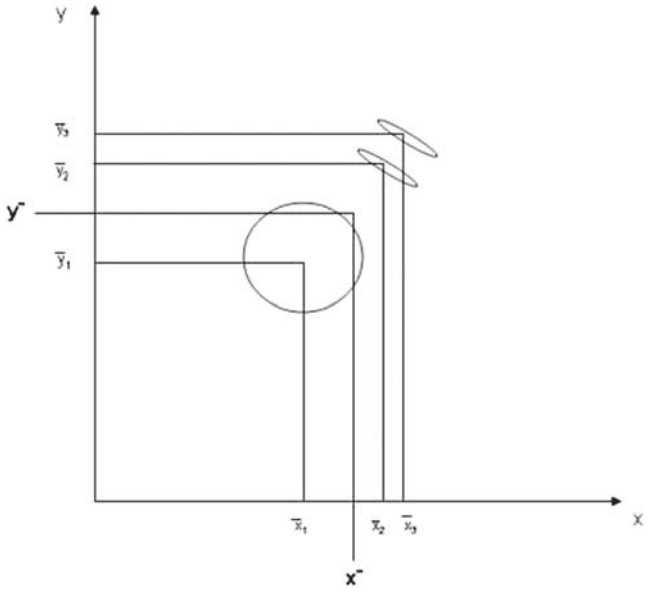

Fig. 18. Centroid calculation.

processed by first thresholding the image and then calculating the area moments.

Once the image has been thresholded, the area moments are calculated and an average or overall centroid is calculated as the location of the focal spot on the sensor.

As shown in Fig. 18, the image of the central flat plate will have a significant "plate blob" of light located at the center of the sensor as the control described in this paper assumes a coarse focus is obtained before the methods of this paper are used for fine focus. If the "plate blob" of light in the center of the image is too big for the area centroids to be calculated, it can be suppressed in the calculation of centroids to obtain locations that are very close to focus.

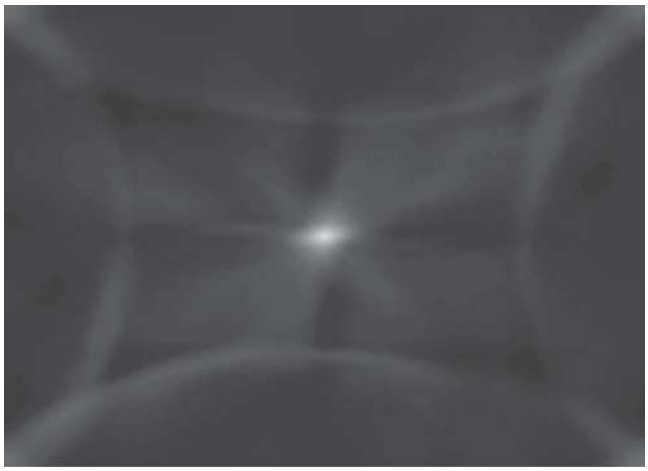

Fig. 19. Correlation up 1 diameter.

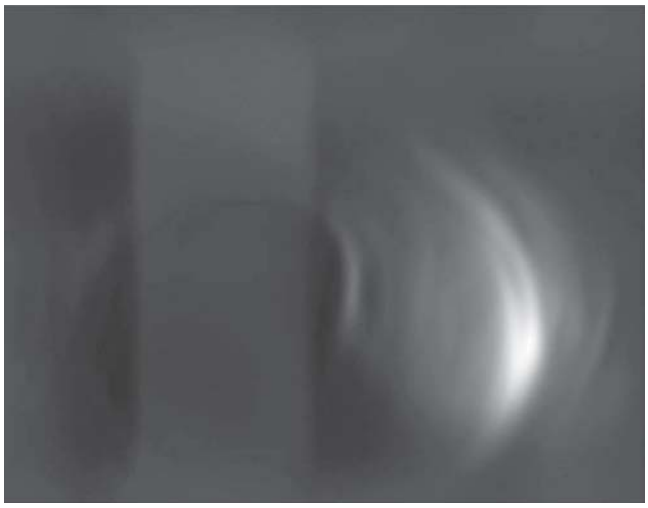

Fig. 20. Correlation 4 diameter offset.

C. ImageJ and Image Analysis

The ImageJ image analysis and processing package from the National Institutes of Health [9, 10] was used to process the images taken in the experiments. The program provides a graphical user interface (GUI) and extensive image analysis commands.

ImageJ performs correlation on images using the conjugate multiplication of the Fourier transforms of two images to be correlated. Masks were utilized to reduce the size of images to include only specific tubes of the absorber area as the region of interest.

Fig. 19 shows the result for the cross-correlation between the images for up 1 diameter from on focus of the solar simulator and the on focus. In this instance, the correlation is smeared and basically located at the center of the image indicating that the 1 diameter misalignment has not been resolved from the on focus situation in which the maximum value is located in the center of the image.

Fig. 20 shows a much better situation for the correlation technique. This figure shows the

Fig. 21. On focus image for area moments.

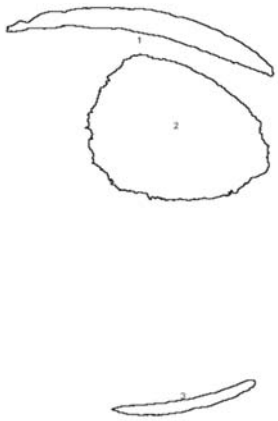

Fig. 22. Particles from 21, blobs 1 and 3 are concentrator images on tubes.

correlation between a 4 diameter misalignment image and the on focus image.

ImageJ was also utilized for the analysis outlined in method two of this paper. The particular command used was the "Analyze Particles" of the Analyze menu. To prepare the images for analysis, each image had to have a threshold applied to them before Analyze Particles would work.

Fig. 21 presents the situation in the process after the image has been cropped and a threshold has been applied. The next step in the process is shown in Fig. 22 when ImageJ has calculated the individual areas based on a minimum size or threshold of 100 pixels. The 100 pixel limit came from the fact that a 100 pixel area reduced the number of areas to work from and was calculated to be 3–5 percent of the approximately 2000 pixels on a tube blob for a fully lit concentrator on focus. Thus we ignored "tube blobs" that were smaller than 100 pixels signifying less than 5 percent of the concentrator lit. Calculations for the image: up0diam_1diam_pos_x_pt5secs_4_aug_2005 gave an average X value of 194.473 and average Y value of 230.12. The method then uses either the centroid of the central "plate blob" of light or the centroid of the on focus image to generate the difference signal used for concentrator control. For the "tube blob" analysis, the difference calculation gives an $|X|$ difference of 64.148 and a $|Y|$ difference of 68.147. By subtracting the focal spot centroids from the centroid of the "blob" a direction of movement towards focus is generated. When there is no central "plate blob" of light in the image, the centroids for X and Y from the on focus image have to be used for delta calculations. These delta calculations would then be used to generate control values for the hexapod controller. Looking at Fig. 23, it can be seen that this method works down to at least 1.5 in off of focus for the solar simulator. That number is associated with 0.15 deg of offset, which is very close to the arbitrary requirement that we control to 0.1 deg.

VII. SUMMARY AND CONCLUSIONS

A system was needed to provide focus control for solar concentrators used in the high temperature environment of terrestrial and space applications. The system discussed in this paper performs this application superbly. A well-known and used method of measuring imperfections in telescopes, Shack-Hartmann wave front sensor and in the current case, an absorber, was modified and algorithms were developed to use in the control portion of the system developed. The algorithms were developed using ImageJ for processing and analyzing the camera images.

	Label	Area	X	Y	Major	Minor	Angle
1	on_focus_pt5secs_4_aug_2005	4343	276.746	29.401	182.604	30.282	166.102
2	on_focus_pt5secs_4_aug_2005	16891	292.18	139.54	160.747	133.908	134.72
3	on_focus_pt5secs_4_aug_2005	1175	304.546	429.943	109.479	13.665	14.483
Averages			291.157	199.628			
4	up0diam_1diam_pos_x_pt5secs_4_aug_2005	6187	185.416	35.906	183.007	43.066	11.87
5	up0diam_1diam_pos_x_pt5secs_4_aug_2005	27247	258.621	161.973	218.615	158.964	120.044
6	up0diam_1diam_pos_x_pt5secs_4_aug_2005	2705	203.531	424.335	166.181	20.733	164.91
Averages			215.856	207.405			
Differences (On – 1diam)			73.301	-7.777			

Fig. 23. Centroid results.

The two algorithms developed were the correlation and the area moment algorithms. Both methods work for locating the focal spot on the sensor down to about 2–3 Sun simulator diameters off of alignment. This amount of misalignment corresponds to 6–9 in off of alignment of the simulator. The 6–9 in of offset corresponds to 0.6 to 0.9 deg of angle of misalignment. Correlation using only 12 fails to work below 1–2 diameters of misalignment. Area moments did better below 1–2 diameters of misalignment. Good focal spot tracking was seen from 5 diameters of misalignment down to 1.5 in of misalignment. The 1.5 in gives about 0.15 deg of misalignment using the 1×2 m concentrator, which is very close to our original arbitrary requirement.

The system as developed in this paper solves the high temperature problem and gives two algorithms to determine focal spot location.

Future work will include automating, using ImageJ, the steps outlined in this paper to control either a model of the concentrator and thruster or an actual concentrator with hexapod and thruster. Also, a combination of both methods should be studied to overcome the limitations of the correlation method. Finally, data should be taken below 1.5 in of misalignment to verify that the method can get to the 0.1 deg of misalignment and improve the control down to 0.02 deg of misalignment where the thruster acceleration could be utilized in the optimization of concentrator location using a combination of phase only correlation (POC) and area moments or a refined area moment method.

REFERENCES

[1] Holmes, M. R.
Ideal performance of off-axis paraboloid concentrators for solar-thermal propulsion.
Presented at the International Solar Energy Conference, San Antonio, TX, Mar. 31–Apr. 13, 1996, 443–449.

[2] Wassom, S. R.
Focus control system for solar thermal propulsion.
Presented at the 2000 International ADAMS User Conference, Orlando, FL, June 19–21, 2000.

[3] Shack, R., and Platt, B. C.
History and principles of Shack-Hartmann wavefront sensing.
Journal of Refractive Surgery, **17** (Sept./Oct. 2001).

[4] Beasley, J. N.
A novel wave front method for tracking terrestrial concentrator focal spot location.
In *Proceedings of the 52nd JANNAF Propulsion Meeting*, May 10–13, 2004.

[5] Wong, R. Y.
Computer Pattern Classification and Scene Matching.
The Faculty Press, California State University, Northridge, CA, 1981.

[6] Dudzik, M. C. (Ed.)
Electro-Optical Systems Designs, Analysis, and Testing (2nd ed.), vol. 4.
Infrared Information Analysis Center Environmental Research Institute of Michigan, 1996; also SPIE Optical Engineering Press, Bellingham, WA.

[7] Tokovinin, A. A.
Tutorial on adaptive optics at CTIO.
Cerro Tololo Inter-American Observatory, July 10, 2001; available at http://www.ctio.naoa.edu/∼atokovin/tutorial/index.html.

[8] Hibbeler, R. C.
Engineering Mechanics, Statistics.
New York: Macmillan, 1978.

[9] Rasband, W. S.
ImageJ.
U.S. National Institutes of Health, Bethesda, MD, 1997–2005; available at http://rsb.info.nih.gov/ij/.

[10] Beasley, J. N.
Computer program for solar concentrator focus control.
In *Proceedings of the 53rd JANNAF Propulsion Meeting*, Dec. 5–8, 2005.

Joseph N. Beasley (M'84) earned the B.S. in electrical engineering from Bradley University, Peoria, IL, in 1985 and the M.S. in electrical engineering from California State University, Northridge, in 1991. He is currently working on the Ph.D.in applied mathematics, through Claremont Graduate University and California State University, Long Beach.

He has worked at the Air Force Research Laboratory since 1991 as an electronics engineer, instrumentation engineer, data acquisition engineer, and test engineer. He also performed research in controlling and positioning solar concentrators as part of his Ph.D. research at Claremont Graduate University and Cal State University, Long Beach.

Michael R. Holmes earned a Ph.D. in physics, specializing in space plasmas, from the University of Kansas, Lawrence, in 1988.

He has worked at the Air Force Research Laboratory since 1989 studying solar-thermal propulsion and other spacecraft propulsion concepts.

Dr. Holmes is a member of the American Physical Society.

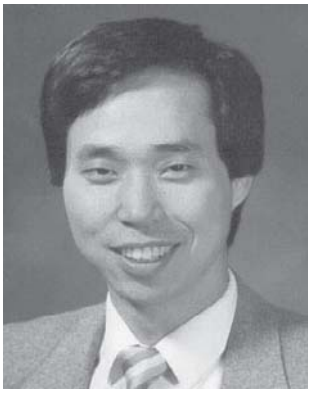

Hen-Geul Yeh (M'82—SM'89) received the Ph.D. degree in electrical engineering and the M.S. degree in mechanical engineering from the University of California, Irvine, in 1982 and 1979, respectively, and the B.S. degree in engineering science, from National Chen Kung University, Taiwan, ROC, in 1978.

He has been with the Electrical Engineering Department at California State University, Long Beach, since 1983, and as professor since 1986. His research activities have included DSP/communication/control algorithms development and implementation using digital signal processors, adaptive filters, wireless local area network, and mobile communications.

Dr. Yeh has been granted three U.S. patents, and received five NASA JPL awards, the Aerospace Corporation Inventor's Award, and an Outstanding Advisor Award of the Best Ph.D. Dissertation, California State University, Long Beach in 1995. He was selected as a NASA JPL Summer Faculty Fellow twice, in 1992 and 2003, respectively. He was selected as Boeing Welliver Faculty Fellow in 2006. He is a registered Professional Electrical Engineer.